Multifrequency Highly Oscillating Aperiodic Amplitude Estimation for Nonlinear Chirp Signal

Anton Emelchenkov, Mathieu Fontaine, Yves Grenier, Hervé Mahé, François Roueff

Multifrequency Highly Oscillating Aperiodic Amplitude Estimation for Nonlinear Chirp Signal

Anton Emelchenkov*†, Mathieu Fontaine†, Yves Grenier†, Hervé Mahé*, François Roueff†
*Valéo PTS, Amiens, France, {anton.emelchenkov,herve.mahe}@valeo.com.
†LTCI, Télécom Paris, Institut Polytechnique de Paris, France, {mathieu.fontaine,yves.grenier,francois.roueff}@telecom-paris.fr.

***Abstract*—This paper addresses the challenge of estimating multiple highly oscillating amplitudes within the nonlinear chirp signal model. The problem is analogous to the mode detection task with fixed instantaneous frequencies, where the oscillating amplitudes signify mechanical vibrations concealing crucial information for predictive maintenance. Existing methods often focus on single-frequency estimation, employ simple amplitude functions, or impose strong noise assumptions. Furthermore, these methods frequently rely on arbitrarily chosen hyperparameters, leading to sub-optimal generalization for a diverse range of amplitudes. To address these limitations, our approach introduces two estimators, based on Capon filters and negative log-likelihood approaches respectively, that leverage locally stationary assumptions and incorporate hyperparameters estimation. The results demonstrate that, even under challenging conditions, these estimators yield competitive outcomes across various noisy scenarios, mitigating the drawbacks associated with existing methods.**

***Index Terms*—chirp signal, amplitude estimation, locally stationary process, filtering, hyperparameters estimation**

I. Introduction

Signal amplitude estimation is a common task with applications in diverse fields such as speech enhancement [1], brain activity monitoring [2], and mechanics vibration studies [3], [4].

Current methods typically focus on constant or slowly varying amplitudes and do not account for highly oscillating amplitudes present in practical applications. For instance, in mechanics the simultaneous tracking of highly-varying amplitudes, known as 'order tracking', is crucial for vibrational analysis in predictive maintenance [5]. A classical model for order tracking representation is the chirp signal, and the amplitude estimation task is broadly categorized into parametric and non-parametric approaches.

In [6], Friedlander *et al.* proposed decomposing amplitudes as a linear combination of parameterized real-valued functions, establishing a relevant theoretical framework using maximum likelihood estimation. Other works, such as [7], [8], and [9], explored various polynomial functions and demonstrated good performance for signals with constant or slowly varying amplitudes. In contrast, [10], [11] used truncated Fourier series for joint amplitude and phase estimation, though such decomposition may be limited to periodic amplitudes.

Non-parametric approaches involve the use of carefully designed filters that emphasize spectral content for linear chirp signals. These methods encompass the Capon filter, also known as the minimum variance distortionless response (MVDR), as introduced in [12]. Additionally, techniques like amplitude and phase estimation of a sinusoid (APES) [13] are employed for a single frequency, while the matched-filterbank approach (MAFI) [14], [15] is applied for multifrequency amplitude estimation. However, it's worth noting that these approaches do not incorporate modelling for non-stationary noise and overlook considerations for time-varying amplitude. Furthermore, spectral analysis-based methods have garnered significant attention, as indicated by [16]. For instance, in the mechanical industry, a spectrogram-based approach known as the Campbell diagram has been widely utilized for order tracking. Nevertheless, the Campbell diagram proves insufficient for addressing non-linear speed evolution, which may arise from unexpected variations in operating conditions, as highlighted by [17].

The exploration of non-linear chirp signals extends to mode detection intending to estimate their instantaneous phases and amplitudes, as discussed in [18] and [19]. Additionally, the application of deep neural networks (DNN) has naturally surfaced for the estimation of amplitude in non-linear chirp signals, as demonstrated in works such as [20] and [21]. However, while [20] focuses solely on constant amplitude estimation, [21] employs convolutional neural networks (CNN) for denoising and utilizes the Wigner-Ville distribution exclusively for estimating a single amplitude.

This paper focuses on the estimation of multifrequency highly oscillating aperiodic amplitude signals with an underlying nonlinear chirp signal. We introduce two approaches based on the frequency of interest. The first is a maximum log-likelihood estimation (MLE) that parameterizes unknown amplitudes using a truncated Fourier series in addition to a low-degree polynomial, compensating for potential non-periodicity. The second approach is a multifrequency locally stationary Capon estimation solved as an optimization problem. We will propose data-driven approaches to select the hyperparameters for all the mentioned methods. The paper is structured as follows: Section II introduces the non-linear chirp signal model and notation. Section III describes state-of-the-art amplitude estimators and our proposed extensions, while Section IV focuses on hyperparameter estimation. In Section V, we conduct experiments on simulated non-linear chirp signals with various noises, followed by concluding remarks in Section VI.

Notation. By convention, a vector in $\mathbb{K}^m$ is seen as a column vector, that is, we identify $\mathbb{K}^m$ to $\mathbb{K}^{m\times 1}$. We use lowercase bold-face symbols to denote vectors and upper case bold-face symbols for matrices. Let $\mathbf{A} \in \mathbb{C}^{m\times n}$ be a complex matrix. We denote by $\mathbf{A}^\top$, $\mathbf{A}^\mathrm{H}$, $\overline{\mathbf{A}}$ the transpose, conjugate transpose and conjugate of matrix $\mathbf{A}$ respectively. Besides, we denote by

Estimator$[H]\{\theta\}$, an Estimator of θ with hyperparameters H.

II. Model description

We consider a continuous-time signal x represented as a sum of K signals of interest, perturbed by an additive noise:

$$x(t) = \sum_{k=1}^{K} s_k(t) + \varepsilon(t), \quad t \in \mathbb{R}. \tag{1}$$

Each of the components s_k is an AM-FM (amplitude-modulated and frequency-modulated) function, commonly referred to in the signal literature as the non-linear chirp mode [18]

$$s_k(t) = a_k(t)\, \cos\left(2\pi\left(\Lambda_k(t) + \phi_k(t)\right)\right). \tag{2}$$

Here, the time-varying amplitude $a_k(t) \in \mathbb{R}^+$ and phase $\phi_k(t) \in [0, 2\pi)$ are unknown real-valued parameters. The instantaneous frequencies are given by the derivatives $\lambda_k(t) := \Lambda_k'(t)$, $k = 1, \ldots, K$ and are of the form $\lambda_k(t) = f_k r(t)$, where f_k is an order and $r(t)$ is the angular speed. Since the f_k's are known and the angular speed is observed, in contrast to the classical mode detection problem, the instantaneous frequency does not need to be estimated. On the other hand, the additive noise may not be white or even weakly stationary, since in real data, it is impacted by the angular speed, which is time-varying. A more plausible assumption is to have discrete samples of ε centred and locally stationary in the sense of [22].

In practice, we do not have access to the continuous process $x(t)$, and observe a finite sample denoted by $\{x[\tau]\}_{\tau=0}^{T} \in \mathbb{R}^{T+1}$, obtained with frequency sampling F_s, that is, $x[\tau] = x(\tau\, F_s)$ for all $\tau = 0, 1, \ldots, T$. We similarly define $s_k[\tau]$, $\varepsilon[\tau]$, $a_k[\tau]$ and $\Lambda_k[\tau]$.

III. Parameters estimation

A. Campbell diagram

The Campbell diagram is the state-of-the-art method for vibrational analysis of mechanical systems [23]. The goal of the method is to estimate the amplitude absolute values at the given frequency trajectories $\boldsymbol{\lambda}_k = \{\lambda_k[\tau]\}_{\tau=0}^{T}$ with $k \in \{1, \ldots, K\}$ over the time samples $\tau \in [0, T]$ using Short-Time Fourier Transform (STFT).

Recall that for a fixed frequency λ and time τ_0 the STFT of the discrete signal $\{x[\tau]\}_{\tau=0}^{T}$ is defined as

$$\widehat{x}[\tau_0, \lambda] = \sum_{\tau=0}^{T} x[\tau] w[\tau - \tau_0]\, \mathrm{e}^{-\,\mathrm{i}\lambda\tau}$$

for some window w, s.t. $w \geq 0$ and $\sum_{\tau=0}^{T} w[\tau] = 1$.

Given a frequency trajectory $\{(\tau\,;\, \lambda_k[\tau])\}_{\tau=0}^{T}$, we can define Campbell diagram as

$$\mathrm{Campbell}[w]\left\{|a_k[\tau]|_{\tau=0}^{T}\right\} := 2|\widehat{x}[\tau, \lambda_k[\tau]]|_{\tau=0}^{T}.$$

In other words, the Campbell diagram is double of the square root of the spectrogram, evaluated at the frequency trajectory $\{(\tau\,;\, \lambda_k[\tau])\}_{\tau=0}^{T}$.

B. Multi-frequency Capon estimator

The single-frequency Capon estimator [12] aims to select the spectral content at a particular frequency λ by filtering the input signal. The optimal finite impulse response (FIR) filter h is designed to minimize the power of its output while ensuring that the filter does not distort the frequency λ [24].

In such an approach we assume that the spectral content of interest is located around λ, whereas the rest is noise. If the valuable spectral content spans multiple frequencies $\{\lambda_1, \lambda_2, \ldots, \lambda_K\}$, it is natural to consider a set of filters

$$\mathbf{H} = \left[\begin{array}{cccc} \mathbf{h}_1 & \ldots & \mathbf{h}_K \end{array}\right] \in \mathbb{C}^{(M+1)\times K},$$

where each of the filters $\mathbf{h}_k \in \mathbb{C}^{M+1}$ highlights a spectral content at a given frequency λ_k, suppressing the content at the other $K-1$ frequencies $\{\lambda_k'\}_{k' \neq k \in \{1,\ldots,K\}}$.

Let $\mathcal{H}_M$ be the set of all FIR filters with support $[-M/2, \ldots, M/2]$. For $h \in \mathcal{H}_M$ we denote by $\mathbf{h}$ the corresponding vector of $\mathbb{C}^{M+1}$ stacking the non-zero filter coefficients from top to bottom. The response of $h \in \mathcal{H}_M$ at frequency λ is given by

$$h^*(\lambda) = \sum_{m=-M/2}^{M/2} h(m)\, \mathrm{e}^{-2\,\mathrm{i}\,\pi\lambda m} = \boldsymbol{\zeta}(\lambda)^{\mathrm{H}}\mathbf{h},$$

where $\boldsymbol{\zeta}(\lambda) = [\mathrm{e}^{i\pi\lambda M}, \ldots, \mathrm{e}^{-i\pi\lambda M}]^\top \in \mathbb{C}^{M+1}$. Single-frequency Capon filter is a FIR filter with a minimal output power with a transfer function equal to one at a frequency λ. It is defined as the solution of the following minimization problem

$$\arg\min_{h \in \mathcal{H}_M} \mathbb{E}\left[|h * x[\tau]|^2\right] \text{ u.c. } \boldsymbol{\zeta}(\lambda)^{\mathrm{H}}\mathbf{h} = 1. \tag{3}$$

To generalize this approach to a time-varying setting with multiple instantaneous frequencies $\{\lambda_1[\tau], \ldots, \lambda_K[\tau]\}$ we propose to use a filter h_k of minimal power with the transfer function equal to one at the frequency of interest $\lambda_k[\tau]$ and zero at the other frequencies $\lambda_{k'}[\tau], k' \neq k$. Therefore,

$$h_k^{opt}[\tau] = \arg\min_{h \in \mathcal{H}_M} \mathbb{E}\,|h * x[\tau]|^2 \text{ u.c. } \mathbf{Z}_{\tau,M}\,\mathbf{h} = \mathbf{e}_k. \tag{4}$$

where $\mathbf{e}_k$ is the k^{th} canonical vector and $\mathbf{Z}_{\tau,M}$ is $K \times (M+1)$ matrix

$$\mathbf{Z}_{\tau,M} = \left[\begin{array}{cccc} \boldsymbol{\zeta}(\lambda_1[\tau]) & \boldsymbol{\zeta}(\lambda_2[\tau]) & \ldots & \boldsymbol{\zeta}(\lambda_K[\tau]) \end{array}\right]^{\mathrm{H}}.$$

To explain the usefulness of the optimal filter h_k^{opt} for estimating $|a_k[\tau]|$, we use that $a_k[\tau']$ and $\phi_k[\tau']$ are approximately constant equal to their values at $\tau' = \tau$ for $\tau' \in [\tau - M/2, \tau + M/2]$. This leads to approximating the signal model (1) *locally* on this interval by

$$x[\tau'] \approx \sum_{k=0}^{K} a_k[\tau] \Re\left[\mathrm{e}^{2\,\mathrm{i}\,\pi\lambda_k[\tau]\,(\tau'-\tau) + 2\,\mathrm{i}\,\pi\Lambda_k[\tau] + \mathrm{i}\,\phi_k[\tau]}\right] + \varepsilon[\tau'].$$

Then for any $h \in \mathcal{H}_M$ satisfying the constraint of (4),

$$h * x[\tau] \approx \frac{a_k[\tau]}{2}\, \mathrm{e}^{2\,\mathrm{i}\,\pi\{\lambda_k[\tau]\,(\tau + M/2) + \Lambda_k[\tau] + \phi_k[\tau]\}} + h * \varepsilon[\tau],$$

It follows that

$$\mathbb{E}\,|h * x[\tau]|^2 \approx \frac{1}{4}\,|a_k[\tau]|^2 + \mathrm{Var}(h * \varepsilon[\tau]). \tag{5}$$

Therefore the argmin in (4) aims to reduce the second term to the smallest possible value and thus recover the first term only, which is the parameter of interest (up to the factor $1/4$).

However, in practice, we do not have access to the expectation in (4) and must solve an empirical version of this optimization problem, which we now derive. Let us define the backward (τ, M)-*local sample*

$$\mathbf{x}^-_{\tau,M} = \left[\; x\left[\tau + \tfrac{M}{2}\right] \quad \dots \quad x\left[\tau - \tfrac{M}{2}\right] \;\right]^\top \in \mathbb{C}^{M+1}$$

from time $\tau + \frac{M}{2}$ back to $\tau - \frac{M}{2}$. Note that, for any $h \in \mathcal{H}_M$, denoting $\mathbf{\Gamma}^-_{\tau,M} = \mathbb{E}\left[\mathbf{x}^-_{\tau,M}\mathbf{x}^{-\mathrm{H}}_{\tau,M}\right]$, we have

$$\mathbb{E}\left[|h * x[\tau]|^2\right] = \mathbf{h}^{\mathrm{H}}\,\mathbf{\Gamma}^-_{\tau,M}\,\mathbf{h}\;.$$

Using Theorem R35 in [24] one can deduce that h_k^{opt} is well defined and problem (4) possess unique solution given by $\mathbf{h}_k^{opt}[\tau] = \mathbf{H}^{opt}_{\tau,M}\,\mathbf{e}_k$, where we set

$$\mathbf{H}^{opt}_{\tau,M} = \left(\mathbf{\Gamma}^-_{\tau,M}\right)^{-1}\,\mathbf{Z}^{\mathrm{H}}_{\tau,M}\,\left(\mathbf{Z}_{\tau,M}\,\left(\mathbf{\Gamma}^-_{\tau,M}\right)^{-1}\,\mathbf{Z}^{\mathrm{H}}_{\tau,M}\right)^{-1}\;.$$

Moreover, the corresponding minimum is $\mathbf{h}_k^{opt}[\tau]^{\mathrm{H}}\,\mathbf{\Gamma}^-_{\tau,M}\,\mathbf{h}_k^{opt}[\tau]$, which reads

$$\mathbf{e}_k^\top\,\left(\mathbf{Z}_{\tau,M}\,\left(\mathbf{\Gamma}^-_{\tau,M}\right)^{-1}\,\mathbf{Z}^{\mathrm{H}}_{\tau,M}\right)^{-1}\,\mathbf{e}_k\;.$$

Hence our Capon estimator follows by replacing $\mathbf{\Gamma}^-_{\tau,M}$ in this expression by its empirical estimate $\widehat{\mathbf{\Gamma}}_{\tau,M,L}$ defined as the $(M+1)\times(M+1)$ Toeplitz matrix associated to the *local empirical auto-covariance function* (see [25]) estimated from the sample $x[\tau']$, $\tau' \in [\tau - L/2, \tau + L/2]$, by

$$\widehat{\gamma}_{\tau,L}(\ell) = \frac{1}{L}\sum_{\substack{\tau_1,\tau_2=0\\ \tau_1-\tau_2=\ell}}^{L} x\left[\tau + \tau_1 - L/2\right]\,x\left[\tau + \tau_2 - L/2\right].$$

Therefore we define the multi-frequency Capon estimator as

$$\frac{1}{2}\sqrt{\mathbf{e}_k^\top\,\left(\mathbf{Z}_{\tau,M}\,\left(\widehat{\mathbf{\Gamma}}_{\tau,M,L}\right)^{-1}\,\mathbf{Z}^{\mathrm{H}}_{\tau,M}\right)^{-1}\,\mathbf{e}_k}\;,$$

denoted by $\mathrm{Capon}[M,L]\{|a_k[\tau]|^T_{\tau=0}\}$ in the following.

C. Maximum likelihood estimator

Note that each of the non-linear chirp modes in (2) can be rewritten as

$$s_k[\tau] = a^c_k[\tau]\cos\left(2\pi\,\Lambda_k[\tau]\right) - a^s_k[\tau]\sin\left(2\pi\,\Lambda_k[\tau]\right),$$

where $a^c_k[\tau] = a_k[\tau]\cos\left(2\pi\phi_k[\tau]\right)$ and $a^s_k[\tau] = a_k[\tau]\sin\left(2\pi\phi_k[\tau]\right)$. The maximum likelihood estimation (MLE) presented further is suited to estimate $a^c_k[\tau]$ and $a^s_k[\tau]$. Having estimated these parameters one can recover $|a_k[\tau]|$ and $\phi_k[\tau] \pm \pi$ by taking the modulus and the argument of $a^c_k[\tau] + \mathrm{i}\,a^s_k[\tau]$. To estimate the unknown parameters $a^m_k[\tau], m \in \{c, s\}$ we approximate them as linear combinations of some well-chosen real-valued functions $[\psi_j[\tau]]_{j=1}^J := \boldsymbol{\psi}[\tau] \in \mathbb{R}^J$.

$$a^m_k[\tau] \approx \sum_{j=1}^{J} \alpha^m_{j,k}\psi_j[\tau] = \left(\boldsymbol{\alpha}^m_k\right)^\top\,\boldsymbol{\psi}[\tau]\;.$$

In the following we choose to take for the vector of functions $\tau \mapsto \boldsymbol{\psi}[\tau]$, a basis of polynomials up to degree J_P jointly with a Fourier basis with fundamental frequencies n/p with $p = \frac{T}{F_s}$ and $n = 1, \dots, J_F$, hence $J = 1 + J_P + 2\,J_F$ and, for $j_p = 0, \dots, J_P$ and $j_f = 1, \dots, J_F$, $\psi_{j_p}[\tau] = \tau^{j_p}$, $\psi_{J_P+2j_f-1}[\tau] = \cos\left(2\pi\frac{j_f}{p}\tau\right)$ and $\psi_{J_P+2j_f}[\tau] = \sin\left(2\pi\frac{j_f}{p}\tau\right)$. We typically use J_P much smaller than J_F. Indeed the quality of a finite Fourier expansion to approximate a given function depends on the smoothness of the corresponding periodic extension and the polynomial part of the approximation aims to smooth out the discontinuities of the derivatives of order up to J_P of this periodic extension at the extreme points of the time interval of observation. Using the previous approximations, we get that

$$x[\tau] - \varepsilon[\tau] \approx \boldsymbol{\alpha}^\top\mathbf{g}[\tau], \tag{6}$$

where vector $\boldsymbol{\alpha} = \left[\left(\boldsymbol{\alpha}^c\right)^\top, \left(\boldsymbol{\alpha}^s\right)^\top\right]^\top \in \mathbb{R}^{2JK}$ with $\boldsymbol{\alpha}^{c/s} = \left[\left(\boldsymbol{\alpha}^{c/s}_1\right)^\top, \dots, \left(\boldsymbol{\alpha}^{c/s}_K\right)^\top\right]^\top \in \mathbb{R}^{JK}$, and, analogously, $\mathbf{g}[\tau] = \left[\mathbf{g}^s[\tau]^\top, \mathbf{g}^c[\tau]^\top\right]^\top$ with

$$\mathbf{g}^c[\tau] = \left[\boldsymbol{\psi}[\tau]^\top\cos(2\pi\,\Lambda_1[\tau]), \dots, \boldsymbol{\psi}[\tau]^\top\cos(2\pi\,\Lambda_K[\tau])\right]^\top,$$

and $\mathbf{g}^s[\tau]$ similarly defined with cosines replaced by sines. Writing Eq. (6) for all $\tau = 0, \dots, T$, we have

$$\mathbf{x} \approx \mathbf{G}\boldsymbol{\alpha} + \boldsymbol{\varepsilon}\;, \tag{7}$$

where $\mathbf{x} = [x[\tau]]^T_{\tau=0} \in \mathbb{R}^{T+1}$, $\boldsymbol{\varepsilon} = [\varepsilon[\tau]]^T_{\tau=0} \in \mathbb{R}^{T+1}$ and $\mathbf{G} = [\mathbf{g}[\tau]]^T_{\tau=0} \in \mathbb{R}^{T+1\times 2JK}$. The MLE is obtained by maximizing the likelihood associated to this model with a Gaussian white noise $\boldsymbol{\varepsilon}$ leading to the linear regression estimator (see [6])

$$\mathrm{MLE}[J_P, J_F]\{\boldsymbol{\alpha}\} = \left(\mathbf{G}^\top\mathbf{G}\right)^{-1}\mathbf{G}^\top\mathbf{x}. \tag{8}$$

This estimator can be used although the noise is not truly Gaussian nor white, a case often referred to as the misspecified case in the statistical literature. Note that the obtained estimator is based on an approximation of the time functions of interest using certain bases expansions hence can also be regarded as a non-parametric regression projection estimator, [26].

IV. Hyperparameters choice

All estimators of Section III depend on hyperparameters, as they need to adapt to the unknown smoothness of the functions $t \mapsto a_k(t)$ and $t \mapsto \phi_k(t)$, $k = 1, \dots, K$ (in addition to the unknown distribution of the noise $n(t)$). For each estimator, the optimal hyperparameters are the ones that minimize the risk (*e.g.* the MSE), the corresponding estimator being referred to as the *oracle estimator*. However computing the MSE requires the ground truth and in practice one has to use empirical

counterparts. We propose two approaches in our context: 1) a *universal* cross validation (CV) criterion which can be applied to all estimators of Section III and 2) the Akaike Information Criterion (AIC) that only applies to the MLE of Section III-C.

A. V-Fold Cross-Validation

We can obtain estimators of $a_k[\tau]$ and $\phi_k[\tau]$, $k = 1, \dots, K$, $\tau = 0, \dots, T$, for each of the methods described in Section III with their respective hyperparameters. We now explain how to compute the CV criterion possibly applicable to any method able to produce such estimators.

As in the V-Fold CV we split the data $D = \{(\tau, x[\tau])\}_{\tau=0}^{T}$ into randomly shuffled train and validation groups $D_{train}(v)$ and $D_{val}(v)$, $v = 1, \dots, V$ so that $\{D_{val}(v)\}_{v=1,\dots,V}$ form a partition of D and $D_{train}(v) = D \setminus D_{val}(v)$. For each v, in the signal formed from $D_{train}(v)$ we replace *missing* values (that fall into $D_{val}(v)$) by zeroes. We obtain a signal $x^{(v)}[\tau]$ and produce estimates $\widehat{a}_k^{(v)}[\tau]$ and $\widehat{\phi}_k^{(v)}[\tau]$, yielding the signal estimates

$$\widehat{s}_k^{(v)}[\tau] = \widehat{a}_k^{(v)}[\tau] \cos\left(2\pi\left(\Lambda_k[\tau] + \widehat{\phi}_k^{(v)}[\tau]\right)\right).$$

Then the cross-validation metric associated to the current method and current hyperparameters is defined as the squared errors between the observed signal and the reconstructed signal averaged on the validation groups:

$$\mathcal{E} = \frac{1}{T+1} \sum_{v=1}^{V} \sum_{(\tau; x[\tau]) \in D_{val}(v)} \left(x[\tau] - \sum_{k=1}^{K} \widehat{s}_k^{(v)}[\tau]\right)^2.$$

B. Akaike Information Criterion for MLE

As explained in Section III-C, Estimator MLE$[J_P, J_F]$ can be interpreted as a Gaussian likelihood maximizer. Observing that for given J_P and J_F, the dimension of the estimated parameter is $\mathrm{d} = 1 + 2K(1 + J_P + 2\,J_F)$ (that is the dimension of $\boldsymbol{\alpha}$ in (7) plus 1 for the dimension of the unknown variance of $n(t)$). It is then straightforward to derive

$$\mathrm{AIC}[J_P, J_F] = 2\,\mathrm{d} + (T+1)\left(\log\left(2\pi \frac{\|\mathbf{x} - \mathbf{G}\widehat{\boldsymbol{\alpha}}\|^2}{T+1}\right) + 1\right),$$

where $\widehat{\boldsymbol{\alpha}} = \mathrm{MLE}[J_P, J_F]\{\boldsymbol{\alpha}\}$ as defined by (8).

V. Numerical Experiments

A. Experimental setup

To evaluate proposed estimators we consider a simulated signal $s[\tau]$ with $K = 4$ highly-oscillated amplitudes and $\phi_k[t] \equiv 0$. $s[\tau]$ is sampled for 10 seconds with frequency $F_s = 10kHz$. The signal $s[\tau]$ is crafted to resemble a real-life vibrational signal, such as the one in Fig. 1.

We compare three different settings where the signal is perturbed by additive noise. These include white Gaussian noise, AR1 noise with a leading coefficient $\varphi = 0.9$, and a noise comprising white Gaussian noise and descending lines. For each of the cases, we consider scenarios with high (SNR = 0dB) and low (SNR = 10dB) levels of noise, where SNR stands for the signal-to-noise ratio $10\log_{10}\frac{\sum_{\tau=0}^{T}\sum_{k=1}^{K}|a_k[\tau]|^2}{\sum_{\tau=0}^{T}|\varepsilon[\tau]|^2}$.

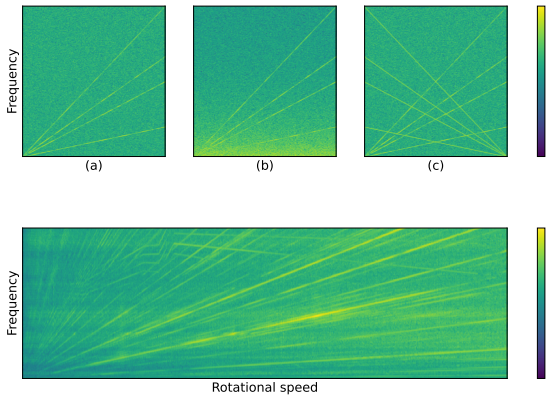

Fig. 1. Upper row: spectrogram of simulated signal perturbed by (a) white noise (SNR = 0dB), (b) AR1 noise (SNR = 0dB), (c) white noise (SNR = 0dB) and descending lines with constant amplitude. Lower row: spectrogram of the vibrational measurements of a gearbox in case of ascending rotational speed. Values and units are omitted for the sake of confidentiality.

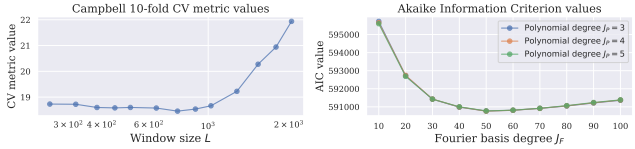

Fig. 2. CV and AIC curves for the white noise setting (SNR = 0dB).

The performance of the estimators is assessed through 100 Monte-Carlo simulations. To choose the optimal hyperparameters for the estimators, we use the universal CV criterion for the Campbell estimator and AIC for the MLE (see Fig. 2 as an example). For MLE we consider polynomial degree $J_P \in \{3, 4, 5\}$ and degree of Fourier basis J_F ranges from 10 to 100 with the step of 10. For Campbell, we use a sliding Hann window of size L between 256 and 2048. We use the Capon estimator with window size L_{CV}, obtained with CV for Campbell estimator, and various covariance matrix sizes M. The Capon estimators displayed in Fig. 3 correspond to $M = 96$ in white noise (0 db setting) and $M = L_{CV}$ in AR noise (0 db setting).

Obtained amplitude estimates $\widehat{a_{k,I}}[\tau]$ are compared via the mean-squared error (MSE) over the $K = 4$ amplitudes, starting at $\tau = \tau_0$

$$MSE_I = \frac{1}{K(T - \tau_0 + 1)} \sum_{k=1,\tau=\tau_0}^{K,T} \left(a_k[\tau] - \widehat{a_{k,I}}[\tau]\right)^2,$$

where $\widehat{a_{k,I}}[\tau]$ is obtained either using the oracle or adaptively chosen hyperparameters by CV or AIC ($I = \mathrm{Oracle/HypOpt}$). To assess the overall estimators' performance in a fair setting, we compute the MSE (Table I) after 1s ($\tau \geq \tau_0$) of signal to avoid extremely close amplitudes at the start of the sample. Note that the Capon estimator is omitted in Table I as its results are comparable to Campbell's. Fig. 3 however investigates amplitude estimation in the first second for all methods.

B. Results and discussion

As we can see from the results of Table I, MLE outperforms the Capon estimator in almost all the cases, providing accurate estimates of highly varying amplitude. It is worth noting a small margin between the oracle estimators and the ones obtained with CV and AIC, indicating the robustness of the

TABLE I
COMPARISON OF THE MSE (MEAN ± STANDARD DEVIATION) FOR MLE AND CAMPBELL ESTIMATORS IN VARIOUS NOISE SETTINGS.

Noise type	SNR	Method	$\text{MSE}_{\text{HypOpt}} \downarrow$	$\text{MSE}_{\text{Oracle}} \downarrow$
White	0 dB	MLE	$\mathbf{0.075}$ $(\pm\mathbf{0.008})$	$\mathbf{0.065}$ $(\pm\mathbf{0.007})$
		Campbell	0.100 (±0.013)	0.085 (±0.008)
	10 dB	MLE	$\mathbf{0.033}$ $(\pm\mathbf{0.007})$	$\mathbf{0.029}$ $(\pm\mathbf{0.002})$
		Campbell	0.044 (±0.005)	0.038 (±0.003)
White + lines	0 dB	MLE	$\mathbf{0.118}$ $(\pm\mathbf{0.011})$	$\mathbf{0.113}$ $(\pm\mathbf{0.011})$
		Campbell	0.169 (±0.022)	0.143 (±0.011)
	10 dB	MLE	$\mathbf{0.092}$ $(\pm\mathbf{0.005})$	$\mathbf{0.083}$ $(\pm\mathbf{0.006})$
		Campbell	0.116 (±0.009)	0.101 (±0.006)
AR1	0 dB	MLE	$\mathbf{0.299}$ $(\pm\mathbf{0.073})$	$\mathbf{0.226}$ $(\pm\mathbf{0.054})$
		Campbell	0.438 (±0.138)	0.282 (±0.052)
	10 dB	MLE	$\mathbf{0.127}$ $(\pm\mathbf{0.028})$	$\mathbf{0.109}$ $(\pm\mathbf{0.022})$
		Campbell	0.193 (±0.044)	0.126 (±0.021)

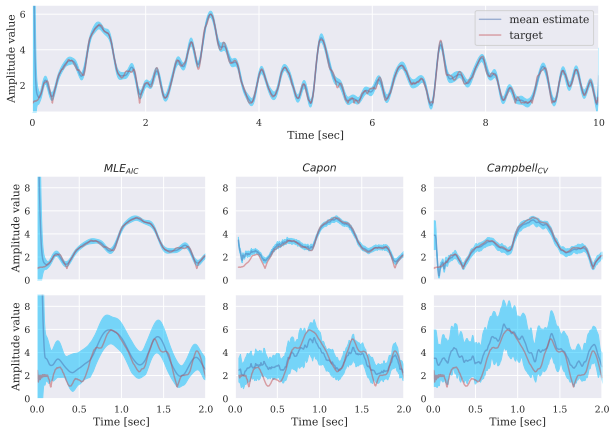

Fig. 3. First row: amplitude ($a_4[\tau]$) estimation with MLE_{AIC} under white noise setting (SNR = 0dB). Second and third rows: close-up comparison of amplitude estimation (first 2 seconds) under various noise settings (SNR = 0dB): (i) estimation of $a_4[\tau]$ under the white noise; (ii) estimation of $a_1[\tau]$ under AR noise.

methods. However, MLE suffers from the explosion at the beginning of the signal, in the ill-posed setting of closely-located amplitudes. To address this, the start of the signal can be effectively estimated by Campbell, and the estimate can be refined by Capon with a properly chosen covariance matrix size M. In the presence of AR noise, Capon accurately captures the signal's shape, resulting in a lower bias in the estimates. Moreover, compared to Campbell_{CV}, Capon and MLE_{AIC} demonstrate lower variance in all the cases.

VI. CONCLUSION

The paper proposes two adaptive methods for the estimation of highly oscillating amplitudes in nonlinear chirp signal with known frequencies. The developed methods show robustness under various noise settings and the ability to accurately estimate non-trivial highly-varying amplitudes. To tune the hyperparameters of the estimators we propose efficient approaches for finding optimal hyperparameters that result in estimators exhibiting performance comparable to that of oracle estimators.

REFERENCES

[1] Y. Tsao and Y.-H. Lai, "Generalized maximum a posteriori spectral amplitude estimation for speech enhancement," *Speech Communication*, vol. 76, pp. 112–126, 2016.

[2] M. Rosenblum, A. Pikovsky, A. A. Kühn, and J. L. Busch, "Real-time estimation of phase and amplitude with application to neural data," *Scientific reports*, vol. 11, no. 1, p. 18037, 2021.

[3] M. Wolf, M. Rudolph, and O. Kanoun, "Amplitude and frequency estimator for aperiodic multi-frequency noisy vibration signals of a tram gearbox," *Journal of Vibroengineering*, vol. 23, pp. 1492–1507, aug 2021.

[4] Y. Yang, Z. Peng, W. Zhang, and G. Meng, "Parameterised time-frequency analysis methods and their engineering applications: A review of recent advances," *Mechanical Systems and Signal Processing*, vol. 119, pp. 182–221, 2019.

[5] S. Lu, R. Yan, Y. Liu, and Q. Wang, "Tacholess speed estimation in order tracking: A review with application to rotating machine fault diagnosis," *IEEE Transactions on Instrumentation and Measurement*, vol. 68, no. 7, pp. 2315–2332, 2019.

[6] B. Friedlander and J. M. Francos, "Estimation of amplitude and phase parameters of multicomponent signals," *IEEE Transactions on Signal Processing*, vol. 43, no. 4, pp. 917–926, 1995.

[7] M. Jabloun, F. Leonard, M. Vieira, and N. Martin, "A new flexible approach to estimate the ia and if of nonstationary signals of long-time duration," *IEEE Transactions on Signal Processing*, vol. 55, no. 7, pp. 3633–3644, 2007.

[8] M. Jabloun, N. Martin, F. Leonard, and M. Vieira, "Estimation of the instantaneous amplitude and frequency of non-stationary short-time signals," *Signal processing*, vol. 88, no. 7, pp. 1636–1655, 2008.

[9] Z. Peng, G. Meng, F. Chu, Z.-Q. Lang, W. Zhang, and Y. Yang, "Polynomial chirplet transform with application to instantaneous frequency estimation," *IEEE Transactions on Instrumentation and Measurement*, vol. 60, no. 9, pp. 3222–3229, 2011.

[10] S. Chen, Z. Peng, Y. Yang, X. Dong, and W. Zhang, "Intrinsic chirp component decomposition by using fourier series representation," *Signal Processing*, vol. 137, pp. 319–327, 2017.

[11] S. Chen, X. Dong, G. Xing, Z. Peng, W. Zhang, and G. Meng, "Separation of overlapped non-stationary signals by ridge path regrouping and intrinsic chirp component decomposition," *IEEE Sensors Journal*, vol. 17, no. 18, pp. 5994–6005, 2017.

[12] J. Capon, "High-resolution frequency-wavenumber spectrum analysis," *Proceedings of the IEEE*, vol. 57, no. 8, pp. 1408–1418, 1969.

[13] J. Li and P. Stoica, "An adaptive filtering approach to spectral estimation and sar imaging," *IEEE Transactions on Signal Processing*, vol. 44, no. 6, pp. 1469–1484, 1996.

[14] P. Stoica, A. Jakobsson, and J. Li, "Matched-filter bank interpretation of some spectral estimators," *Signal Processing*, vol. 66, no. 1, pp. 45–59, 1998.

[15] P. Stoica, H. Li, and J. Li, "Amplitude estimation of sinusoidal signals: survey, new results, and an application," *IEEE Transactions on Signal Processing*, vol. 48, no. 2, pp. 338–352, 2000.

[16] Q. He, E. Wu, and Y. Pan, "Multi-scale stochastic resonance spectrogram for fault diagnosis of rolling element bearings," *Journal of Sound and Vibration*, vol. 420, pp. 174–184, 2018.

[17] P. Bonello, "The extraction of campbell diagrams from the dynamical system representation of a foil-air bearing rotor model," *Mechanical Systems and Signal Processing*, vol. 129, pp. 502–530, 2019.

[18] Q. Chen, L. Xie, and H. Su, "Multivariate nonlinear chirp mode decomposition," *Signal Processing*, vol. 176, p. 107667, 2020.

[19] X. Tu, J. Swärd, A. Jakobsson, and F. Li, "Estimating nonlinear chirp modes exploiting sparsity," *Signal Processing*, vol. 183, p. 107952, 2021.

[20] H. Su, Q. Bao, and Z. Chen, "Parameter estimation processor for chirp signals based on a complex-valued deep neural network," *IEEE Access*, vol. 7, pp. 176278–176290, 2019.

[21] G. Ben, X. Zheng, Y. Wang, N. Zhang, and X. Zhang, "A local search maximum likelihood parameter estimator of chirp signal," *Applied Sciences*, vol. 11, no. 2, p. 673, 2021.

[22] R. Dahlhaus, "Locally stationary processes," in *Time Series Analysis: Methods and Applications* (T. Rao, S. Rao, and C. Rao, eds.), vol. 30 of *Handbook of Statistics*, pp. 351–413, North Holland, 2012.

[23] M. P. Boyce, *Gas turbine engineering handbook*. Elsevier, 2011.

[24] P. Stoica, R. L. Moses, *et al.*, *Spectral analysis of signals*, vol. 452. Pearson Prentice Hall Upper Saddle River, NJ, 2005.

[25] F. Roueff and A. Sánchez-Pérez, "Prediction of weakly locally stationary processes by auto-regression," *ALEA : Latin American Journal of Probability and Mathematical Statistics*, vol. 15, pp. 1215–1239, 2018.

[26] A. B. Tsybakov, *Introduction to nonparametric estimation*. Springer Series in Statistics, New York: Springer, 2009. Revised and extended from the 2004 French original, Translated by Vladimir Zaiats.